Methylamine's effects on methylglyoxal-containing aerosol: chemical, physical, and optical changes.

David O. De Haan,*[1] Aki Pajunoja,[2] Lelia N. Hawkins,[3] Hannah G. Welsh,[3] Natalie G. Jimenez,[1] Alexia De Loera,[1] Melanie Zauscher,[1+] Alyssa D. Andretta,[1] Benjamin W. Joyce,[1] Audrey C. De Haan,[1] Matthieu Riva,[4§] Tianqu Cui,[4] Jason D. Surratt,[4] Matthieu Cazaunau,[5] Paola Formenti,[5] Aline Gratien,[5] Edouard Pangui,[5] Jean-François Doussin[5]

[1]Department of Chemistry and Biochemistry, University of San Diego, 5998 Alcala Park, San Diego CA 92110 USA

[2]Department of Applied Physics, University of Eastern Finland, P.O. Box 1627, 70211 Kuopio, Finland

[3]Department of Chemistry, Harvey Mudd College, 301 Platt Blvd, Claremont CA 91711 USA

[4]Department of Environmental Sciences and Engineering, Gillings School of Global Public Health, The University of North Carolina at Chapel Hill, Chapel Hill, NC, 27599 USA

[5]Laboratoire Interuniversitaire des Systèmes Atmosphériques (LISA), UMR7583, CNRS, Université Paris-Est-Créteil (UPEC) et Université Paris Diderot (UPD), Institut Pierre Simon Laplace (IPSL), Créteil, France

[+]Currently at California Air Resources Board, 1001 I St., Sacramento, CA 95814

[§]Currently at Université de Lyon, Université Claude Bernard Lyon 1, CNRS, IRCELYON, F-69626, Villeurbanne, France

*Corresponding_Author, ddehaan@sandiego.edu

ABSTRACT. Methylamine, a common atmospheric amine species, is found in the gas, particle, and aqueous phases. It has been shown to form light-absorbing, oligomeric species in reactions with methylglyoxal and other aldehyde species in bulk aqueous-phase experiments and when mixed into seed aerosol as a sulfate salt. Here we explore the influence of multiphase methylamine chemistry on aerosol production, properties, and molecular composition. When methylglyoxal aerosol particles were exposed to ~2 ppm methylamine gas in a humid chamber, rapid browning was observed, but not growth. Aerosol bounce measurements indicated that particles became slightly more viscous and hydrophobic upon methylamine exposure. Subsequent cloud processing increased both viscosity and hygroscopicity, but had little effect on browning, consistent with high-resolution mass spectrometry results showing that aerosol oligomer dicarbonyl functional groups were transformed into cationic imidazole rings. Photolytic cloud processing triggered the incorporation of hydryoxyacetone and acetal radicals into oligomers. Since dicarbonyl species are a major component of atmospheric aerosol particles, these results suggest that methylamine exposure and cloud processing will slowly increase brown carbon content, viscosity, and hygroscopicity of atmospheric aerosol.

Keywords: brown carbon, viscosity, hygroscopicity, bounce fraction, imidazoles, oligomers

Introduction

The reaction of water-soluble gases in clouds and aqueous aerosol particles is an important source of secondary organic aerosol material,[1, 2] especially in the free troposphere.[3] The particles formed via aqueous-phase pathways ("aqSOA"), like other types of aerosol particles, can strongly affect human health[4] and global climate.[5] The atmospheric formation of light-absorbing brown carbon (BrC) aerosol is of increasing interest given the potential of BrC to increase temperatures in the atmosphere and at the Earth's surface through the direct aerosol effect.[6-8]

Layers of brown carbon aerosol may also reduce photochemistry at lower altitudes.[9] Aqueous reactions between dicarbonyl species (*e.g.*, glyoxal and methylglyoxal) and ammonia or amine species form light-absorbing, nitrogen-containing oligomer species over many hours in bulk aqueous solutions,[10-13] and may be significant sources of secondary brown carbon.[11, 14, 15]

Dicarbonyl[16-19] and amine species[20-22] are found in the gas, particulate, and aqueous phases in the atmosphere, but their multi-phase chemistry is not captured in bulk-phase experiments. For example, aerosol reactions between dicarbonyls and amino acids are orders of magnitude faster than in bulk-phase experiments,[23, 24] and the rapid formation of oligomerized products can significantly increase aerosol particle viscosity to form semi-solids.[25] Our recent study of ammonium sulfate and methylammonium sulfate aerosol measured browning upon exposure to gas-phase methylglyoxal that was as fast as the 1-min timescale of chamber mixing, but it was unclear whether subsequent addition of methylamine gas caused any further browning.[24] Updyke *et al.* showed that lab-generated SOA browns on a filter when exposed for 3 days to 100 ppb of NH_3 gas,[26] but the effects of aerosol exposure to gas-phase amines to our knowledge have not been systematically explored.

Here we describe three complementary types of multiphase experiments exploring the effects of methylamine on methylglyoxal-containing aerosol: 1) direct-to-filter aerosol browning experiments involving aqueous droplets containing ammonium sulfate, methylglyoxal, and methylamine, the latter two of which may evaporate; 2) cloud chamber experiments where methylglyoxal (oligomer) aerosol were exposed to gas-phase methylamine while particle phase, size distribution, and optical properties were continuously monitored *in situ*, and 3) small chamber experiments where browning was measured as a function of RH as methylglyoxal/AS particles were exposed to methylamine gas. Major aerosol-phase chemical species were

identified in a subset of cloud chamber experiments by high-resolution mass spectrometric analysis of filter extracts. We find that, although methylglyoxal aerosol particles do not increase measurably in size when exposed to gas-phase methylamine and subsequent cloud processing, the particles quickly become more viscous, hygroscopic, and light-absorbing, especially below 400 nm, due to the formation of cationic N-containing oligomeric species.

Methods

Reagents were used as received from Sigma-Aldrich unless otherwise mentioned. Stock solutions were generated by dilution of methylamine (40% w/w), methylglyoxal (Alfa-Aesar, 40% w/w), glycine (>99%) or AS (>99%) in deionized water (>18 MOhm).

Filter experiments comparing aerosol vs bulk browning simulations of the concentrated aqueous aerosol phase were performed on 0.3 M mixtures of methylglyoxal, amine (methylamine or glycine), and AS. (See Scheme S1 in Supplemental Information.) After recording the absorption spectrum of the freshly mixed solution, the solution was atomized (TSI 9302) in 1.5 L/min dry, particle-free air. Atomized droplets were diffusion-dried to relative humidity (RH) < 10%, then collected on pre-weighed Teflon membrane filters (Tisch, 1.0 μm pore size, 47 mm diam.). After 4 h of particle collection, the absorption spectrum of the atomizing solution was again recorded. Filters (including blanks) were weighed and analyzed within 30 min of collection by reflectance UV-Vis spectroscopy (JASCO SLM-468 / V-570) before and after ultrasonic extraction (5 min in 5 mL d.i. water). Because filtered aerosol particles of a related system (glyoxal + methylamine + ammonium sulfate) browned during storage (Figure S1), all filters in the experiments described in this section were extracted (5 min sonication in water) and analyzed by UV/vis absorption

spectroscopy as quickly as possible (within 30 min of collection). Absorbance (Abs) in the extract and atomization solutions was converted to mass absorption coefficients using equation (1),

$$\text{MAC (cm^2/g)} = \frac{2.303\ \text{Abs}}{\text{bC}} \quad (1)$$

where b = pathlength in cm and C is the concentration of organics in the extract or solution in g/cm^3. For extracts, C = filter mass increase / extract volume, which assumes that the entire aerosol mass on the filter is extracted.

The CESAM large chamber at LISA is a 4.2 m^3 temperature-controlled, stirred, stainless steel chamber with solar simulator lamps monitored by temperature, pressure and flow sensors.[27] The chamber is held just above ambient pressure using flows of high-purity oxygen and liquid nitrogen boil-off at a respective 20/80 v/v ratio. Gas phase contents were monitored by RH sensors, long-path Fourier-transform infrared spectroscopy (FTIR, Bruker Tensor 37, 192m path length),[27] and high-resolution proton transfer reaction mass spectrometry (PTR-MS, KORE Tech. Series II, inlet temperature 100°C, proton transfer reactor P = 1.64 mbar, glow discharge P = 1.94 mbar, PTR entry voltage = 400 V, E/N ratio = 130). Polydisperse particles were nebulized (TSI 3076 atomizer) from 1-100 mM methylglyoxal solutions into the chamber. These particles were then continuously sampled from the central volume of the chamber through a 1 m Nafion drying tube to scanning mobility particle sizing (SMPS, TSI, 20 – 1000 nm) and cavity-attenuated phase shift single-scattering albedo spectrometers (450 nm CAPS-ssa, Aerodyne). A particle-into-liquid sampler (PILS, Brechtel Manufacturing), located downstream from a denuder with activated carbon strips, also collected chamber aerosol (diluted 1:1 with N_2) into a capillary waveguide UV/vis spectrometer (LWCC-100, 0.94m pathlength) with a pre-column filter to prevent clogging by insoluble material. Dried aerosol were periodically size-selected and sampled for bounce measurements to determine phase transitions vs. RH.[24, 28] Methylamine gas (Fluka, >99%) was added by gas syringe through a septum into the inlet N_2 flow. The chamber was humidified by

additions of expansion-cooled water vapor.[27] The RH in the chamber was subsequently stabilized by routing the inlet N_2 flow through a temperature-controlled bubbler containing high purity water. Cloud events[29] were monitored by extinction of a 633 nm laser beam (central volume) and droplet spectrometer (Palas Welas Digital 2000, 0.5 to 15 μm, sampling from flange of chamber).[27] CAPS-ssa extinction and scattering signals were zeroed against filtered inlet flow every 5 to 15 min to eliminate gas-phase signals, and averaged to SMPS scan frequency. SMPS number and concentrations and PTR-MS signals were corrected for dilution caused by flows into the chamber. The SMPS size distribution was also corrected for wall losses.

After CESAM experiments ending with ≥15 μg/m^3 aerosol concentrations, cloud-processed aerosol were collected for ~14 h at 16 L min^{-1} onto Teflon filters (Tisch, 1.0 μm pore size).[30] Chemical characterization of the particles was performed by ultra-performance liquid chromatography / high-resolution quadrupole time-of-flight mass spectrometry with electrospray ionization (UPLC/ESI-HR-Q-TOFMS; 6520 Series, Agilent) operated in negative and positive ion modes.[30] Filters were extracted by sonicating in methanol (LC-MS Chromasolv-grade, Sigma-Aldrich). The extracts were blown dry under N_2 and reconstituted in 150 μL 50:50 (v/v) methanol:water (>18.2 MΩ) mixture. Five and 10 μL aliquots were injected onto the column (Waters ACQUITY UPLC HSS T3 column, 2.1 × 100 mm, 1.8 μm particle size) and eluted at 0.3 mL min^{-1} with methanol and water, each containing 0.1% acetic acid (negative ion mode) or 0.1% ammonium acetate (LC-MS Chromasolv-grade, Sigma-Aldrich, positive ion mode). Since nitrogen-containing oligomer standards were not available, caffeine (> 99 %, Sigma-Aldrich) served as a surrogate quantification standard for positive ion mode signals.[30]

In small chamber experiments (Scheme S2), a 300 L collapsible Tedlar chamber was filled with dry, particle-free air. Water vapor was added by passing the airflow over water-saturated

vermiculite. Chamber contents were monitored by RH sensor (Vaisala 337 at the point of sampling), SMPS (TSI 3080/3787, 2 L/min sheath flow, 0.2 L/min sample flow) and CAPS-ssa. After these instruments sampled the particle-free chamber, 30 – 300 mM AS + methylglyoxal mixtures were atomized, diffusion dried, neutralized (NRD U500), and added to the chamber. In all chamber experiments, CAPS signals were kept below 1000 Mm^{-1} by routing some inlet flow through a parallel filtered line when necessary. Methylamine gas was added by evaporating a droplet of 40% w/w solution in a heated glass bulb, flowing it with dry air into the chamber to achieve a peak concentration of ~2 ppm.

Results and Discussion

Direct-to-filter experiments: drying of methylglyoxal / amine / AS aerosol. After collecting diffusion-dried methylglyoxal/amine/AS particles onto Teflon filters for 4 hours, the filters were pale yellow in color (for both methylamine and glycine runs). Over 85% of the reflective loss between 240 and 570 nm, and 89% of the integrated reflective loss at all wavelengths, was removed by the 5 min aqueous ultrasonic extraction of each filter (*e.g.* Figure S2). The UV/visible absorption spectra of the extracts, expressed as mass absorption coefficients (MAC), are compared to spectra of the solutions used to generate the aerosol in Figure 1. Methylglyoxal + glycine + ammonium sulfate aerosol particle extracts (lower panel) are at least 10× more light absorbing than the corresponding bulk solution at all wavelengths > 315 nm, and ~20× more light-absorbing above 400 nm. The observation of more extensive brown carbon formation in drying aerosol particles relative to bulk-phase solutions is similar to a previous study of glyoxal + AS mixtures,[31] and was attributed to a combination of concentration effects and the conversion of dicarbonyl dihydrate to the reactive monohydrate at aerosol surfaces.[23]

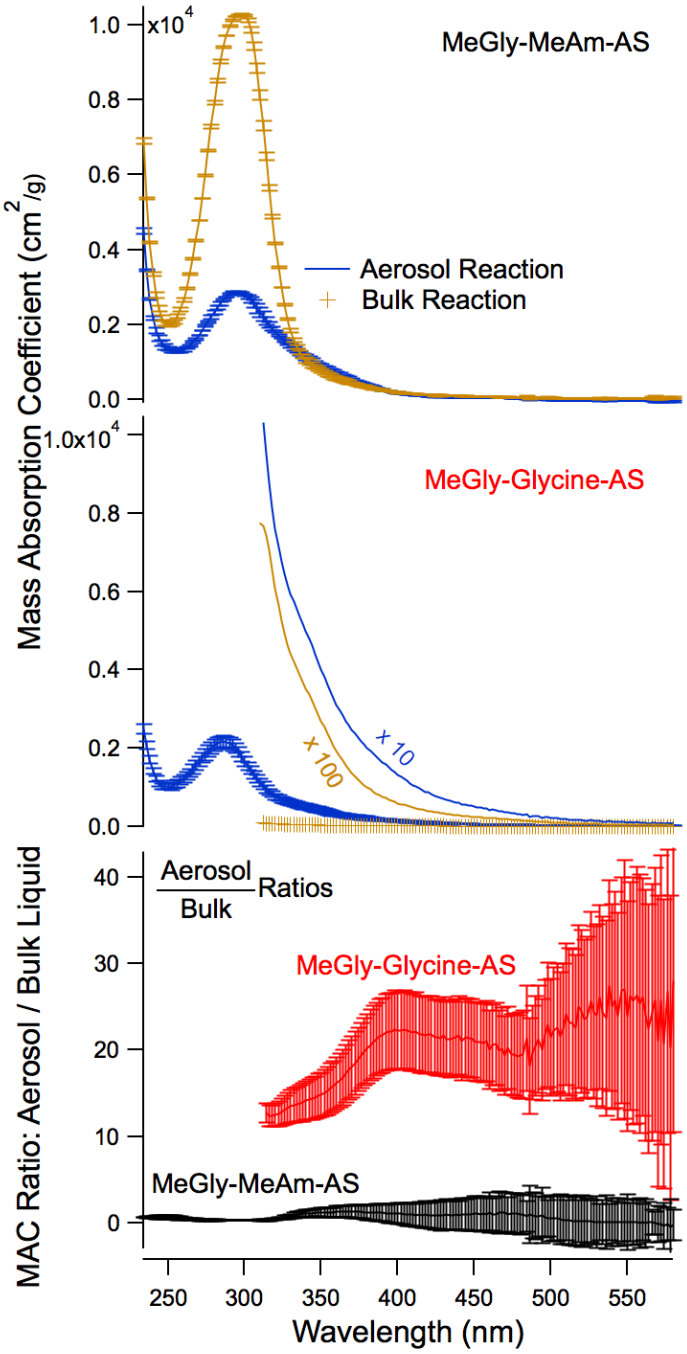

Figure 1: Average mass absorption coefficients of bulk solutions (gold) and aerosol filter extracts (blue) collected from (top) 0.3M methylglyoxal + methylamine + ammonium sulfate and (middle) 0.3M methylglyoxal + glycine + ammonium sulfate experiments with identically-scaled left y-axes. Low wavelength bulk data are cut off in the middle panel due to off-scale absorbance of undiluted bulk solution. Bottom: aerosol / bulk MAC ratios for the two systems. All error bars are ± 1σ for n = 2 to 4 experiments.

When glycine is replaced with methylamine, the methylglyoxal – amine – AS aerosol extract MAC values (upper panel) are almost unchanged. In contrast, the methylamine-containing bulk solution is ~100× more light-absorbing than with glycine, and now has MAC values equal to or greater than the aerosol extracts at all wavelengths. These methylamine bulk solution results are not atmospherically relevant, however. It is likely that higher pH caused by unbuffered methylamine (pH = 7.7) caused rapid browning in these bulk solutions, as has been observed with glyoxal / formaldehyde / amino acid mixtures.[32] In the aerosol experiments, on the other hand, unreacted and unprotonated methylamine molecules will simply evaporate, resulting in lower, atmospherically-relevant pH – and less browning. These experimental results highlight the necessity of studying brown carbon formation chemistry involving methylamine in aerosol-phase experiments, where multiphase processes are unrestricted. In the next sections, we describe multiphase experiments focused on the exposure of methylglyoxal-containing particles to gas-phase methylamine.

CESAM large chamber experiments. *Filter analysis summary.* Experiments at the CESAM chamber (summarized in Table 1) probed the effects of methylamine uptake, cloud processing, and simulated solar irradiation on product distributions, particle phase, and brown carbon formation in seed aerosol particles containing methylglyoxal. Table 1 shows the weighted average of the molecular masses detected by UPLC/ESI-HR-Q-TOFMS in filter extracts collected in Expts 2-5, assuming equal ionization efficiency for this calculation. The average molecular mass of aerosol-phase products is larger in these experiments (where methylglyoxal was added in the aerosol phase) than in previous experiments on the same chemical system where methylglyoxal was added in the gas phase.[24, 30] These larger-mass oligomers are detailed below.

Table 1: Response of MeGly Aerosol to Gas Phase Methylamine Addition: Large Chamber Experiments

Expt	$[MeAm]_g$ (ppm)	$[MeGly]_p$ ($\mu g/m^3$)	%RH at MeAm addition	No bounce %RH (pre-MeAm)	No bounce %RH (post-MeAm)	Minimum albedo reached	MW (avg)
1 (dark)	12 $\mu g/m^3$ pre-mixed MeAm / MeGly aerosol[a]		74 - 96	na	75%[a]	0.83	na
2 (dark)	2.0	320[b]	79%	77%	80%	0.92	238
3 (no clouds)	2.0	200[b]	76	77	82%	0.95	255
4	2.0	380[b]	72	na	84%[c]	0.93	216
5 (low N)	<0.05	330[b]	na	79%	na	0.95	208
6 (dark)	2.0	20,[d] added after $MeAm_{(g)}$	72	na	83%	0.88	na
7 (dark)	2.0	150[b]	77	na	83%	0.905	na
8 (dark)	pH 3.4 $(MeAm)_2SO_4$ aerosol[e]	160[b]	na	76%	na	0.95	na

Notes: **a**: Solution containing 1 mM methylamine and methylglyoxal (pH 4.7) atomized to form aerosol with density = 1.62 ±0.04.[38] **b**: Atomized from 100 mM methylglyoxal solution, pH 4.4, to form aerosol with density = 1.9 ±0.2.[34] **c**: after 30 min photolysis. **d**: Atomized from 10 mM methylglyoxal solution, pH 3.7. **e**: Solution containing 0.1 mM methylamine acidified to pH 3.4 with sulfuric acid atomized to form seed aerosol, added to chamber 80 min after MeGly seed addition. **na**: No measurement.

Exact masses of 48 ions detected in Expt 2-5 filter extracts by UPLC/ESI-HR-Q-TOFMS and their assigned formulae are listed in Table S1; proposed structures corresponding with assigned formulae are shown in Schemes 1 and S3. Thirty-three of the detected ions can be divided among four formation pathways: products of a photolysis-driven pathway involving acetyl radicals,[30] an aldol oligomer pathway involving hydroxyacetone and methylglyoxal,[11, 33, 34] a methylglyoxal self-reaction aldol condensation pathway,[35] and a set of imidazole products,[23, 36-39] including many

imidazoles derived from methylglyoxal aldol oligomers. The three largest peaks detected in these experiments, responsible for 30% of total peak area, *m/z* 183 ($C_9H_{14}N_2O_2$), 361 ($C_{18}H_{20}N_2O_6$), and 111 ($C_6H_{11}N_2$), are imidazoles. Imidazoles were responsible for 44% of detected peak areas, larger than the other three product groups combined. (It must be noted that imidazoles are not necessarily the most abundant product on a concentration basis, given their efficient ionization by ESI.) Photolysis pathway products make up a smaller fraction of total peak areas in Experiments 3 – 5 (20-40%) than in previous experiments (87%) where methylglyoxal gas was added to methylaminium sulfate aerosol.[30] However, gas phase methylglyoxal concentrations are higher in the current work. The different relative amounts of photolysis pathway products in these studies is therefore likely due to the formation of additional particle-phase products via the methylglyoxal aldol and imidazole pathways in the current work.

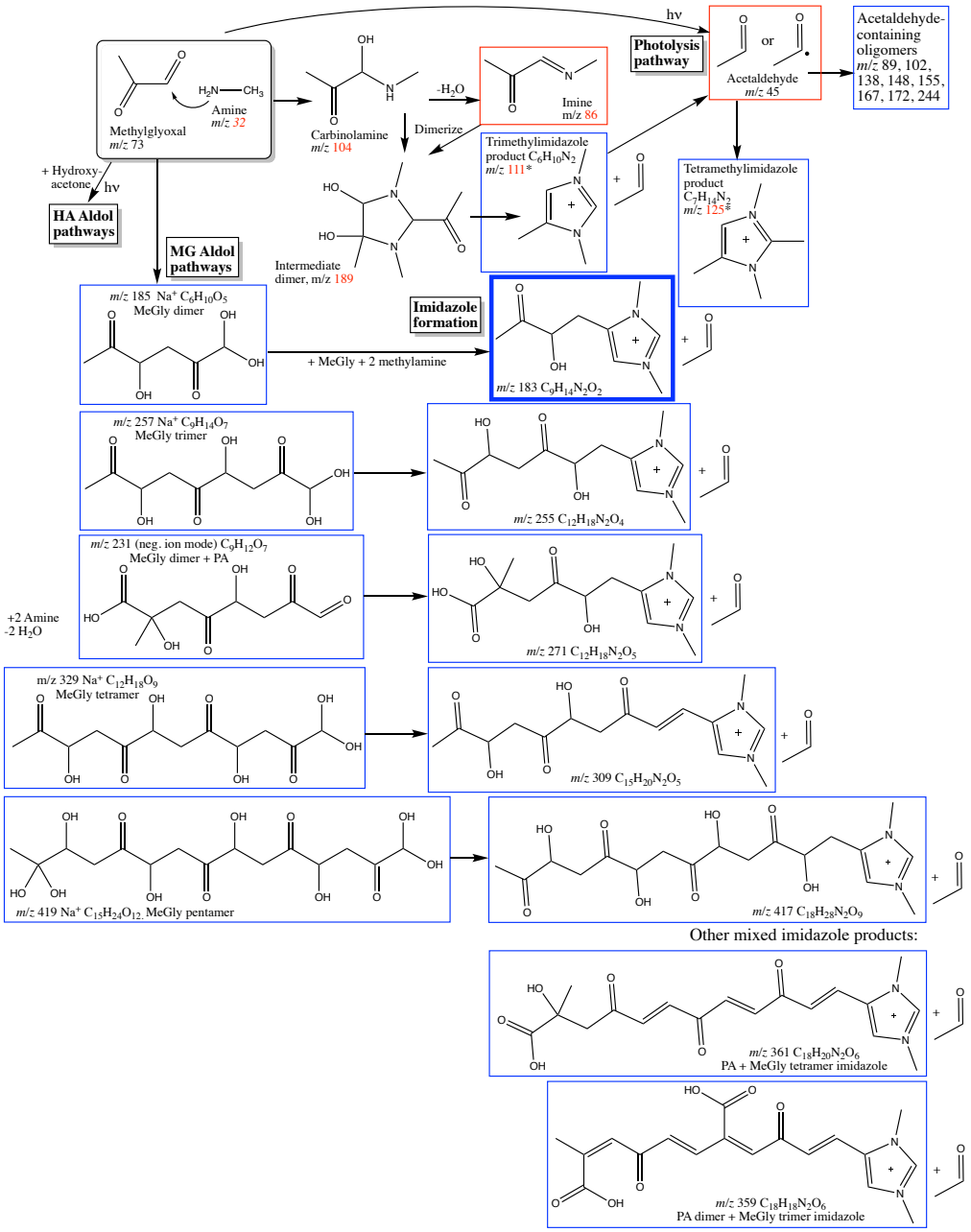

Scheme 1: proposed chemical structures corresponding to product masses detected in Experiments 2-5, formed in methylglyoxal aldol oligomer and imidazole formation pathways (left and right side of scheme, respectively). Blue boxes: detected in aerosol phase by off-line UPLC/ESI-HR-Q-TOFMS filter analysis. Red boxes: detected in gas phase by PTR-MS monitoring. The thick blue box designates methylglyoxal dimer imidazole (*m/z* 183), the largest observed product peak. Previously identified hydroxyacetone aldol and photolysis pathways[30] are shown in Scheme S3. Methylglyoxal dimer (*m/z* 185)[11] and products with *m/z* < 150 were also reported earlier.[30]

Figure 2 shows how yields of each product group differ between Expts. 2-5. As expected, products in the "photolysis" group are present in very low amounts in dark Expt 2, while imidazoles and methylglyoxal oligomers are present in the highest amounts in the dark. Similarly, imidazoles are formed in low amounts in the low-methylamine Expt 5, while nitrogen-free methylglyoxal oligomer yields are not affected. These outcomes increase confidence in our proposed structures and formation pathways. In addition, the pattern of relative yields of hydroxyacetone + methylglyoxal oligomers across Expts. 2-5 are similar to the photolysis-related products, suggesting that the hydroxyacetone incorporated into oligomers is photolytically produced from methylglyoxal in the aerosol phase.

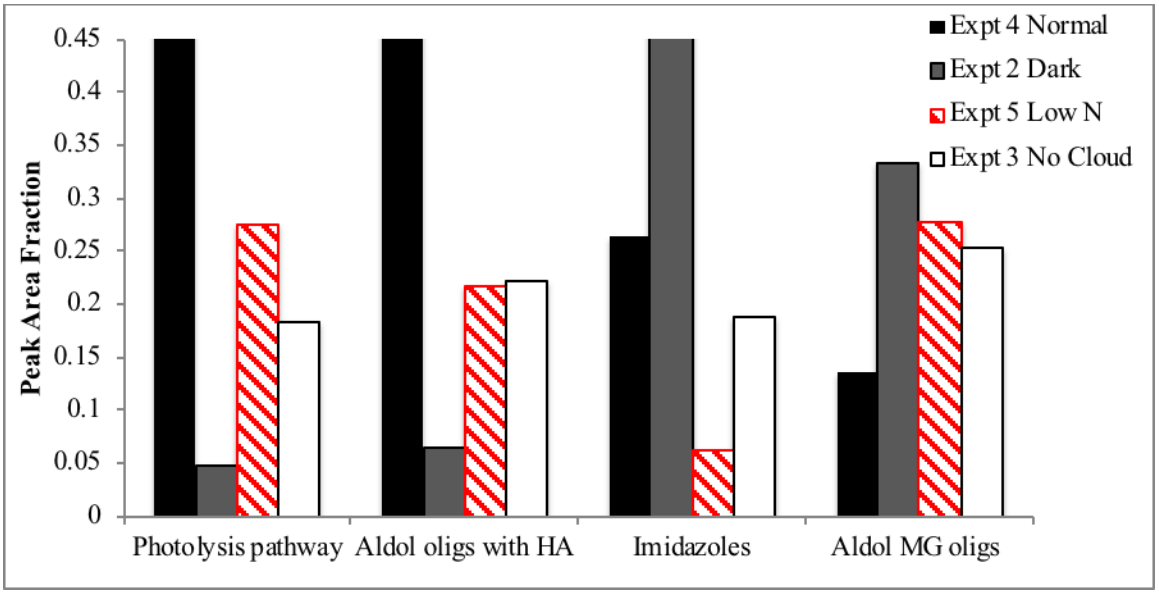

Figure 2: Effect of chamber conditions on products observed, by class. The quantities of each class of products are normalized to a sum of 1 across the four experiments. A class that produced the same total peak area in each experiment would have four equal bars at 0.25, regardless of ionization efficiency. A bar larger than this indicates preferential production under that experimental condition. "Normal" conditions include photolysis, methylamine addition, and 1 or more cloud events.

Although the aerosol filters used to generate this mass spectral dataset were collected over many hours at the end of each experiment, differences between Expts 2-5 suggest how aerosol-phase chemistry responds to chamber events at shorter timescales. For example, in the dark, methylglyoxal aerosol contains mostly aldol oligomers, but the addition of methylamine derivatizes these oligomers with cationic imidazole rings, especially after dark cloud processing. After photolysis, and especially after photolytic cloud processing, acetyl radicals and hydroxyacetone are incorporated into oligomers. To better understand the effects of these processes on the physical and optical properties of aerosol particles, we now look at online measurement data from a larger set of chamber experiments.

Methylglyoxal / methylamine aerosol. Figures 3 and S3 show data from Experiment 1 where a fresh aqueous mixture of 1.1 mM methylamine and 1.0 mM methylglyoxal was used to generate chamber aerosol. This mixture turned a faint yellow during aerosol addition. Consequently, unlike methylglyoxal aerosol, which had an initial albedo $\geq$ 0.94 at 450 nm in all experiments, methylglyoxal / methylamine aerosol was significantly more light-absorbing, with single-scattering albedo = 0.84 after aerosol addition was complete. Although the release of methylglyoxal and imine product was detected in the gas phase by PTR-MS during aerosol addition to the chamber, no methylamine evaporation was observed during the experiment, suggesting that methylamine reacted rapidly and completely in the aqueous phase. Indeed, in the absence of gas-phase methylamine, no further browning of the methylglyoxal/methylamine aerosol occurred: after 4 dark cloud events, albedo had risen from 0.84 to 0.88, and the value of the imaginary component of the index of refraction (k_{imag}) declined slightly from 0.011 to 0.008 ±0.002. However, post-cloud bounce fractions of dried and rehumidified aerosol were higher

when measured between 40 and 60% RH, and lower at RH > 60% (Figure S4). Both of these statistically significant changes were observed whenever methylglyoxal aerosol was cloud-processed in the presence of methylamine gas (*e.g.*, Expts. 2 and 4 in Figure 4). Higher bounce fractions at moderate RH indicate higher particle viscosity,[40] while lower bounce fractions observed only at high RH suggest more hygroscopic surfaces.[41] Thus, we conclude that cloud processing enhances the formation of oligomeric cationic imidazole products that increase particle viscosity and hygroscopicity, but absorb less 450 nm light than their precursor species.

Methylglyoxal aerosol + methylamine (g). When methylglyoxal aerosol was added to a humid chamber already containing methylamine gas (Experiment 6, Figure S5), the aerosol became noticeably light-absorbing at 450 nm (post-baseline albedo = 0.91 ±0.01, post-baseline k_{imag} = 0.008 ±0.001). The aerosol had to be humidified to 80% RH rather than 74% RH before the bounce fraction declined to near zero (Figure S6), indicating that methylglyoxal aerosol exposed to methylamine gas is less hygroscopic than pre-mixed methylgyoxal / methylamine aerosol. This likely indicates that the formation of cationic imidazoles is greater in pre-mixed solutions. In both cases, cloud processing increased bounce fractions at low and medium RH and decreased them at high RH, symptomatic of particles becoming more oligomerized and hygroscopic due to cationic imidazole product formation.

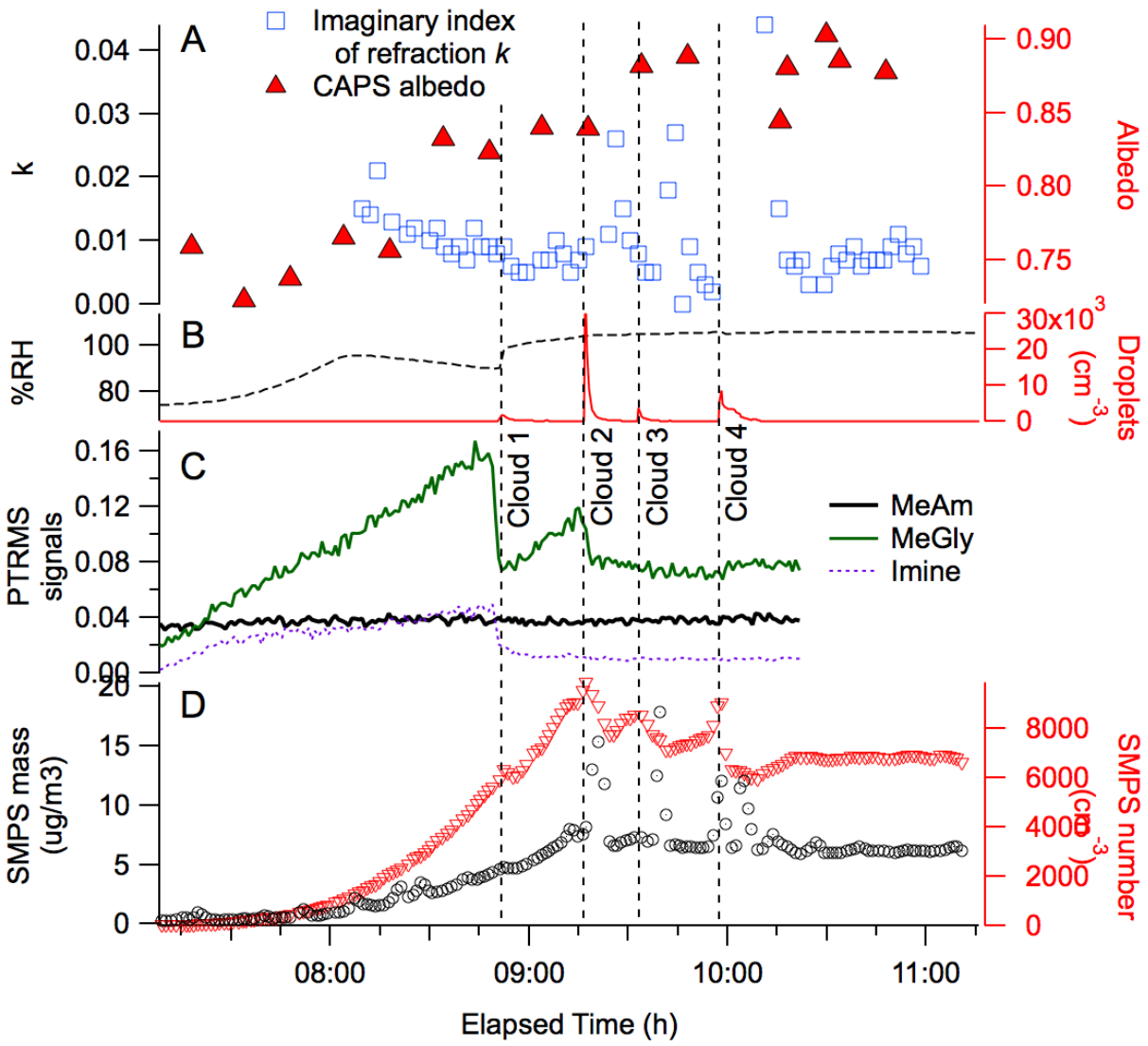

Figure 3: Summary of methylglyoxal / methylamine aerosol Experiment 1. Panel A: Single-scattering albedo measured by CAPS-ssa at 450 nm after each instrument baseline (red triangles), and imaginary index of refraction at 450 nm calculated from CAPS and SMPS data (blue squares). CAPS extinction and scattering data shown in Figure S3. B: chamber RH and cloud droplet counts (traces color-coded to axes). C: Dilution- and water-corrected PTR-MS traces for gas-phase methylglyoxal (m/z = 73, green line, signal of 1 = 350 ±180 ppb), methylamine (m/z = 32, black line, signal of 1 = 970 ±190 ppb, at clean chamber background level for this ion), and imine product (m/z = 86, purple dots). D: Wall loss and dilution-corrected SMPS number density and particulate mass (using aerosol density = 1.62, 74 to 882 nm diam. range, traces color-coded to axes). Cloud events 1-4 (vertical dashed lines) are labeled. Aerosol addition ended just prior to Cloud 2.

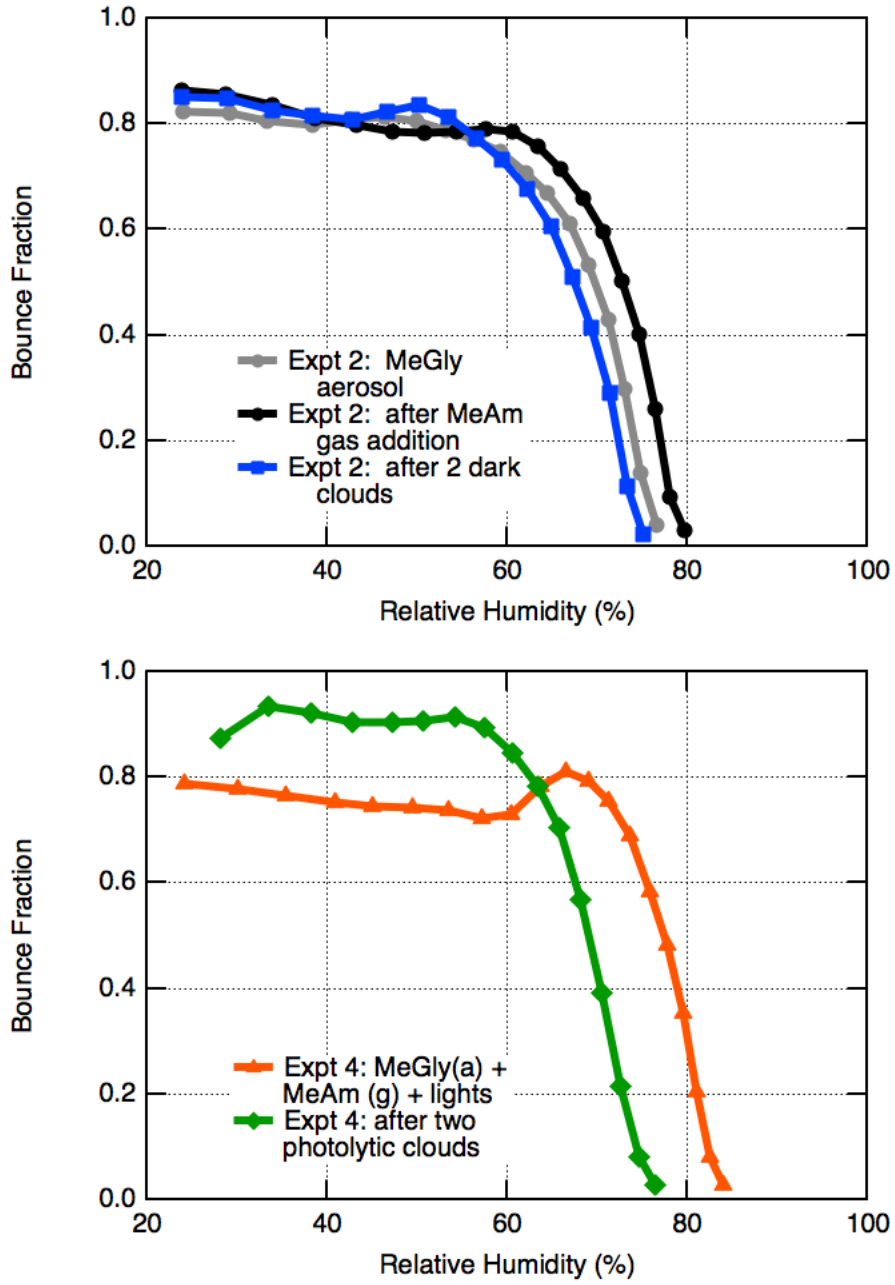

Figure 4: Experiment 2 (upper panel): Black open circles: initial MeGly aerosol. Black filled circles: after ~2 ppm methylamine gas added. Blue squares: after two dark cloud events. The error bars of these three datasets are non-overlapping at RH > 65% (see Figure S4). Experiment 4 (lower panel): Red triangles: MeGly aerosol + ~2 ppm methylamine gas + 30 min photolysis. Green diamonds: after 2 photolytic cloud events. All error bars fit within line widths shown.

In terms of particle browning at 450 nm, cloud processing had opposite effects in the two experiments: in methylglyoxal aerosol placed in a chamber with methylamine gas, browning was enhanced after the first cloud event, with albedo declining from 0.91 to 0.88, k_{imag} increasing from 0.008 ±0.001 to 0.013 ±0.002, and MAC values between 350 and 500 nm reaching the highest values of any experiment. While methylamine signals were constant at background levels during cloud processing of pre-mixed methylglyoxal / methylamine aerosol (Figure 3), in Experiment 6 (Figure S5), methylamine PTR-MS signals declined by nearly 30% within 15 min of cloud event 1. Since the Henry's coefficient of methylamine is only (0.9 ±0.4) mol m^{-3} Pa^{-1},[42] and since PTR-MS methylamine signals did not recover promptly upon cloud droplets evaporation, the observed methylamine uptake must be reactive in nature. Thus, these observations suggest that cloud processing of methylglyoxal aerosol in the presence of gas-phase methylamine caused reactive uptake of methylamine resulting in the combined formation of ionic imidazoles *and* brown carbon products.

In other experiments, methylamine gas was added to the chamber after methylglyoxal aerosol, allowing comparison of methylglyoxal aerosol properties before and after methylamine addition. For example, in Experiment 3 (Figures 5 and S7), the addition of ~2 ppm methylamine gas to the dark, humid chamber did not change dried SMPS particle diameters, but tripled MAC values in the PILS-collected aerosol, lowered albedo at 450 nm by -0.011, and increased $k_{imag\ 450}$ from 0.006 to 0.007, all indicative of aerosol browning without growth. In both Experiments 2 and 3 (Figures 4 and 6, respectively), aerosol bounce fractions increased, most notably above 55% RH. This suggests that methylamine exposure, which initially replaces aldehydes with methylated imine functional groups, may produce a more hydrophobic aerosol surface until cloud processing converts these imine precursors into cationic imidazoles (which make the surface hygroscopic).

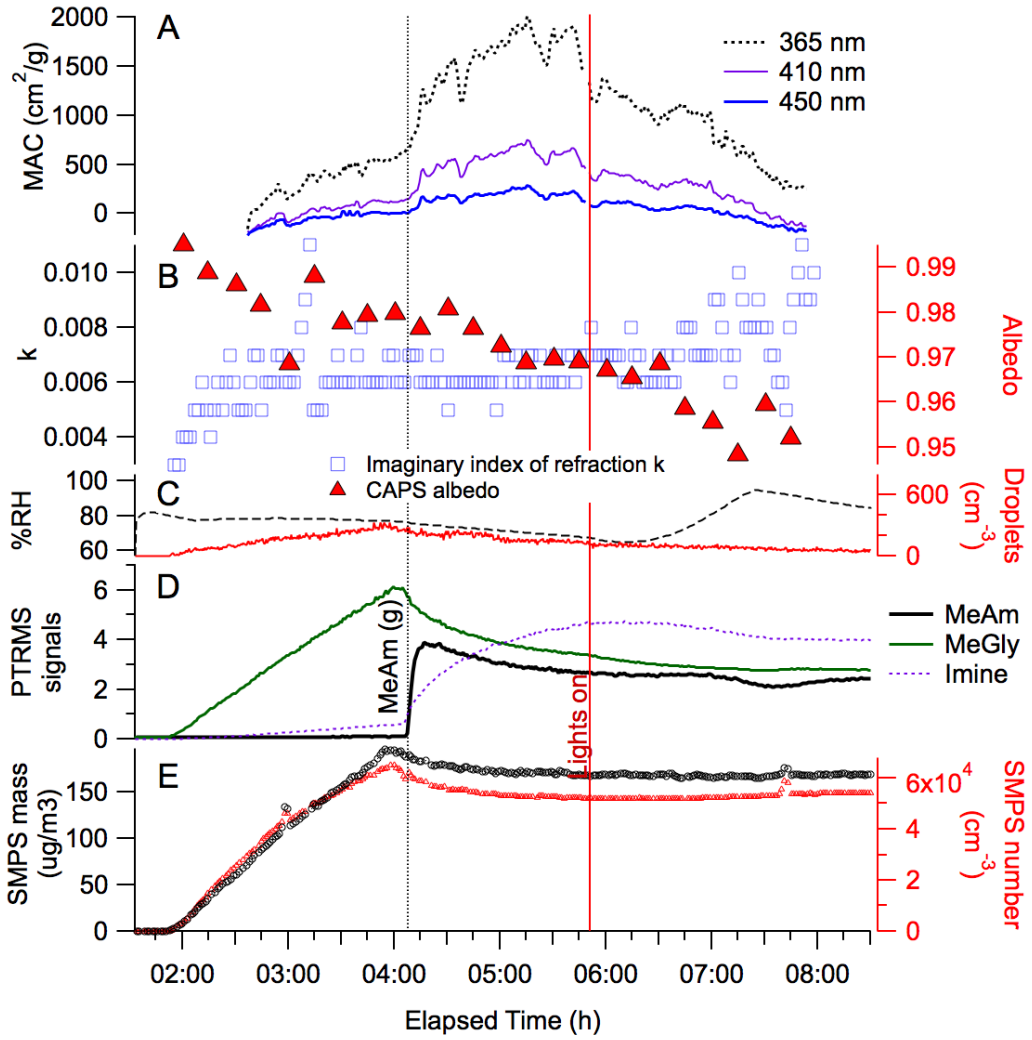

Figure 5: Methyl-glyoxal aerosol + methylamine gas Experiment 3. Panel A: mass absorption coefficients of PILS outflow at 365 nm (dotted black line), 410 nm (thin purple line) and 450 nm (thick blue line). See Figure S7 for full spectra. Panel B: single-scattering albedo measured at 450 nm by CAPS after each instrument baseline (red triangles), and imaginary index of refraction at 450 nm calculated from combined CAPS and SMPS data. Panel C: chamber RH and cloud droplet counts with traces color-coded to axes. Panel D: dilution- and water-corrected PTR-MS traces for gas-phase methyl-glyoxal (m/z = 73, green line, signal of 1 = 350 ±180 ppb), methylamine (m/z = 32, black line, signal of 1 = 970 ±190 ppb), and imine product (m/z = 86, purple dots). Panel E: wall loss and dilution-corrected SMPS number density and particulate mass (using aerosol density = 1.9, 74 to 882 nm diam. range), with increasing number density before t = 4 h indicating addition of MeGly seed aerosol. Additions of methylamine gas (vertical dotted line) and the beginning of photolysis (red line) are labeled.

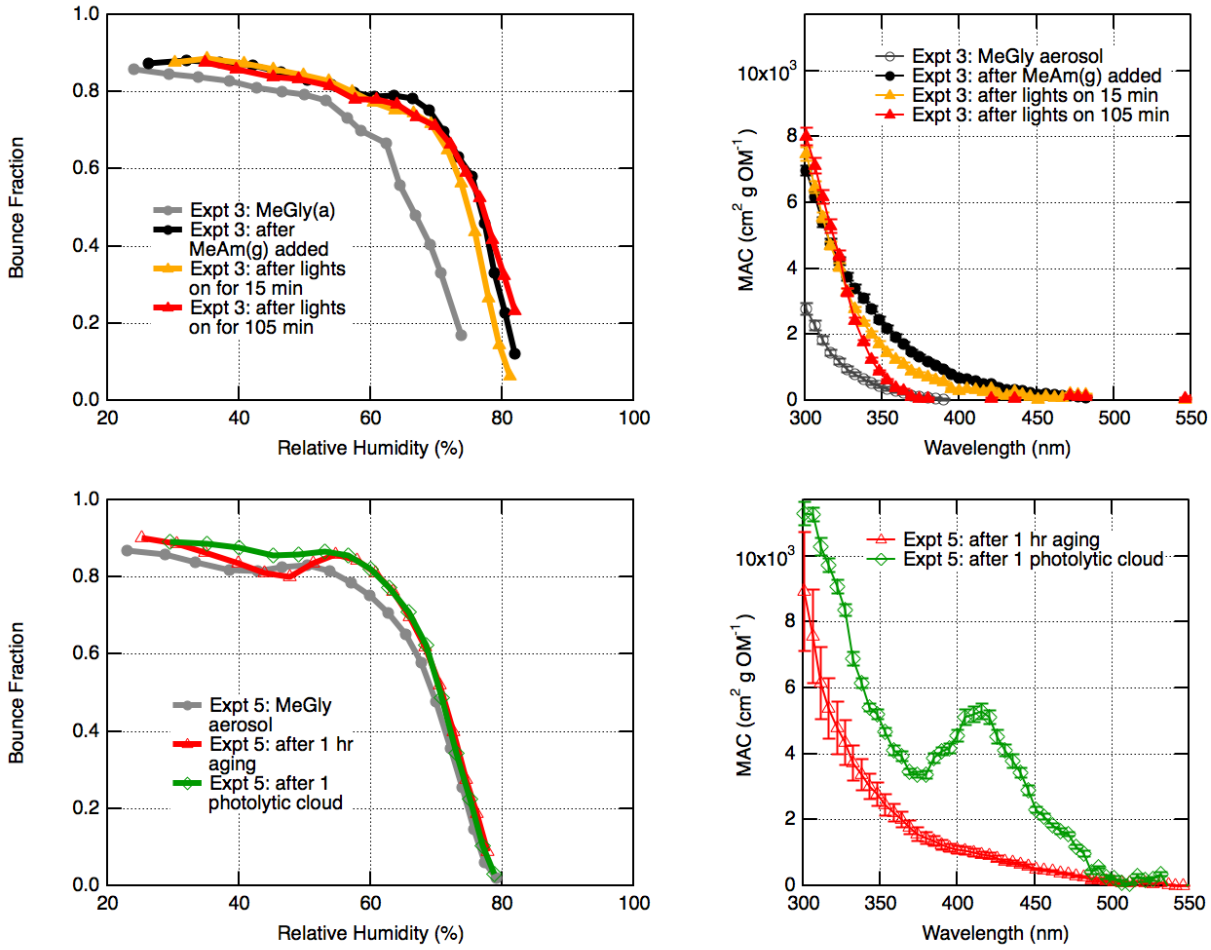

Figure 6: Bounce factors (left) and mass absorption coefficients (right) measured for dried and rehumidified 150 nm particles nebulized from 100 mM methylglyoxal solution sampled from humid CESAM chamber, with the following treatments. Experiment 3 (top panels): Black open circles: initial MeGly aerosol. Black filled circles: after 2 ppm methylamine gas added. Yellow triangles: after 15 min photolysis. Red triangles: after 90 min additional photolysis. Experiment 5 (no methylamine, bottom panels): Black circles: initial MeGly aerosol. Red triangles: aged 1 h. Green diamonds: after photolytic cloud. All error bars in bounce fraction measurements fit within line widths shown.

When the chamber was illuminated by solar simulator lamps after t = 5.8 h in Experiment 3 (Figure 5), MAC values of the aerosol particles sampled by PILS declined, returning to pre-

methylamine levels after 90 min, consistent with photobleaching.[43-45] At the same time, the post-baseline albedo of Nafion-dried particles declined, indicating browning, but only after chamber RH increased to 74%. Particle bounce fractions rapidly fall off beyond this RH, suggesting that aerosol particles undergo a semi-solid to liquid phase change at this point. It appears that drying these aqueous aerosol particles in the CAPS sampling line quickly forms new, conjugated products that are more light-absorbing at 450 nm than the molecules that were photolyzed in the chamber. It is significant that many of the proposed product structures in Scheme 1 could become even more conjugated, and therefore light-absorbing, upon H_2O loss.

For methylglyoxal aerosol exposed to methylamine, cloud-free photolysis had a negligible effect on bounce fractions measured below 60% RH, and above 60% RH the small initial decrease in bounce fraction tends to disappear at longer photolysis times (Figure 6 Expt. 3). However, photolytic cloud processing (Figure 4 Expt. 4) had dramatic effects on bounce fraction, producing aerosol with the highest bounce fractions below 65% RH (0.92) observed in any experiment, while slightly lowering the albedo at 450 nm by ~0.013 (Figure S8). These observations are consistent with photolysis triggering rapid, radical-initiated formation of conjugated oligomers in evaporating cloud droplets[30] via "photolysis" and "HA aldol" pathways, thereby increasing the viscosity of the resulting dried aerosol particles. At the same time, photolytic cloud processing caused the zero-bounce fraction RH to decline from 83 to 76%, again indicating an increase in hygroscopicity. We note (Figure 2) that imidazoles' product fraction after dark *or* photolytic cloud processing is higher than in cloud-free experiments. Thus, formation of imidazoles may explain the increase in hygroscopicty caused by both types of cloud processing.

In Experiment 7 (Figures 7 and S9), methylamine gas was added twice (at t = 3:18 and 6:20 h), before and after a dark cloud event. In the hour after each addition, mass absorption coefficients

of PILS-sampled aerosol rose by factors of 3 and 2, respectively, while no increase in SMPS diameter was observed. Browning after the first methylamine addition appears to be near the detection limit of CAPS-ssa measurements: single-scattering albedo at 450 nm decreased by < 0.01, as MAC_{450} values reached 1000 cm^2/g. (For a clearer drop in albedo after methylamine addition, see Expt. 2 / Figure S10.) Aerosol bounce measurements (Figure S6) show that dark cloud processing increased aerosol viscosity and hygroscopicty as usual, consistent with production of cationic imidazoles. Brown carbon production increased further after the second methylamine addition: MAC_{450} values reached 2400 cm^2/g, and CAPS albedo decreased by an easily measurable 0.028, even as aerosol bounce measurements indicate no further increase in hygroscopicity, perhaps due to a surface already saturated with cationic imidazoles after cloud processing.

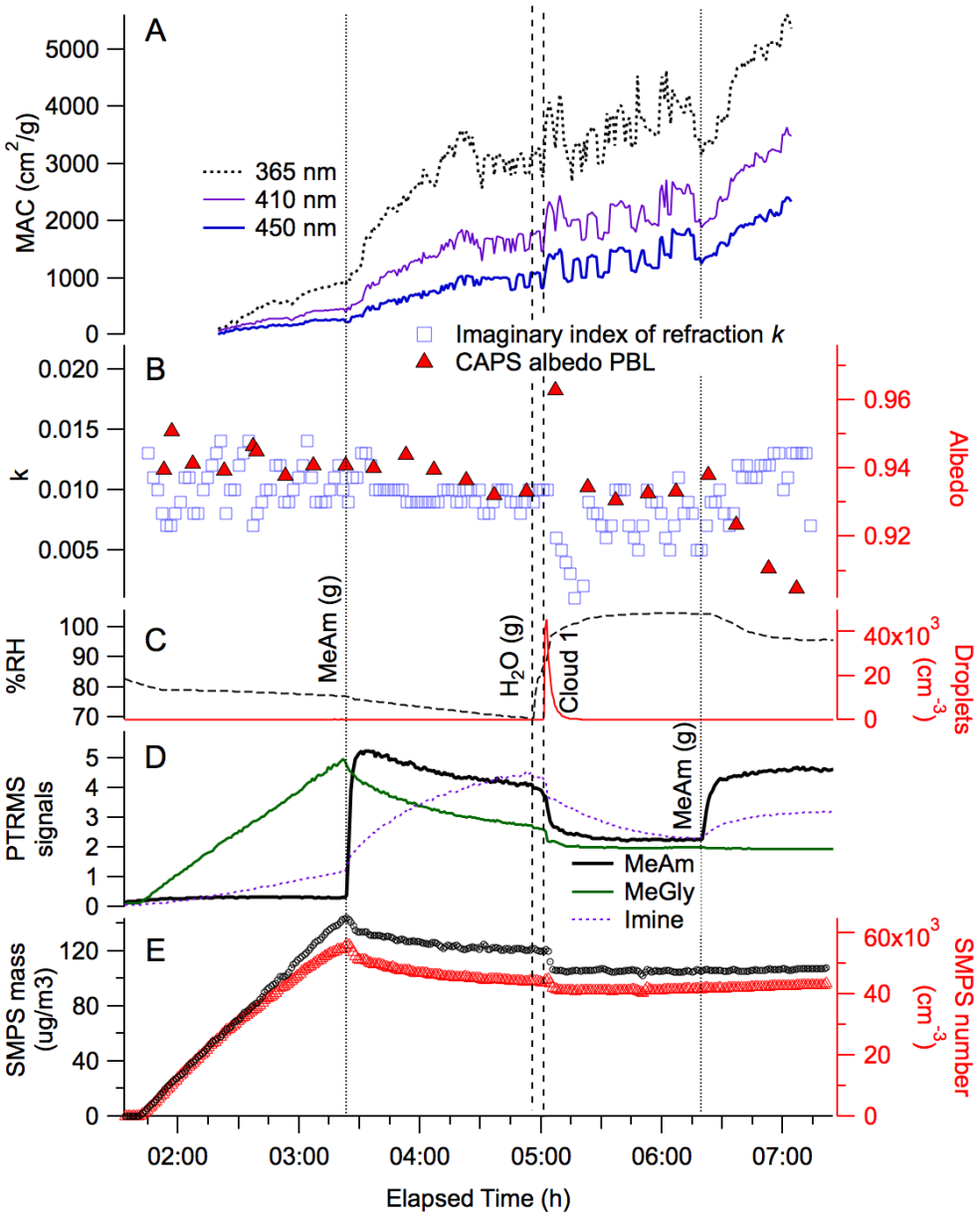

Figure 7: Methylglyoxal aerosol + methylamine gas dark Experiment 7. Panel A: mass absorption coefficients of PILS outflow at 365 nm (dotted black line), 410 nm (thin purple line) and 450 nm (thick blue line). See Figure S9 for full spectra. Panel B: : single-scattering albedo measured at 450 nm by CAPS after each instrument baseline (red triangles), and imaginary index of refraction at 450 nm calculated from combined CAPS and SMPS data. Panel C: chamber RH and cloud droplet counts shown with traces color-coded to axes. Panel D: dilution- and water-corrected PTR-MS signals for gas-phase methylglyoxal (m/z = 73, green line, signal of 1 = 350 ±180 ppb), methylamine (m/z = 32, black line, signal of 1 = 970 ±190 ppb), and imine product (m/z = 86, purple dots). Panel E: wall loss and dilution-corrected SMPS number density and particulate mass (using aerosol density = 1.9, 74 to 882 nm diam. range), with increasing number density before t = 3.5 h indicating addition of MeGly seed aerosol. Additions of methylamine gas (vertical dotted lines), water addition and a cloud event (vertical dashed lines) are labeled.

In Experiment 5, a control experiment with methylamine levels at least 40× lower than other experiments, methylglyoxal aerosol was aged in the chamber for 2 h, photolyzed, and cloud-processed. Without much methylamine present in the aerosol or gas phase, the RH required to drive the bounce fraction of methylglyoxal aerosol to zero does not change during the experiment (Figure 6 bottom), consistent with the idea that hygroscopicity increases in other experiments were caused by cationic imidazoles. Only minor increases in bounce fraction are observed at lower RH, and most of these increases occurred as methylglyoxal aerosol age in the chamber, before photolytic cloud processing. Albedo (at 450 nm in dried chamber aerosol) was near constant during photolysis and photolytic cloud processing (Figure S11), but PILS-sampled aerosol shows an absorbance peak at 410 nm growing in (Figures S11 and S12), accelerating with photolysis and cloud processing. This peak was not observed in experiments where methylamine gas was added, nor has it been observed in methylglyoxal + AS aqueous mixtures,[11] but did appear in Experiment 8 (Figure S12) where methylamine sulfate aerosol was externally mixed with methylglyoxal aerosol in the dark. Nemet *et al.*[46] observed an absorbance band at 430 nm in non-aqueous methylglyoxal solutions, and attributed it to unhydrated α-dicarbonyl functional groups. Such functional groups should always be at least partially hydrated in the aqueous-sampling PILS system, however. It is more likely that the absorbance at 410 nm is due to a MG oligomer with conjugated double bonds. One such dimer, $C_6H_8O_4$ (structure (2) below), was detected at *m/z* 143 by negative ion mode UPLC/ESI-HR-Q-TOFMS in Experiment 2 (the only filter analyzed in negative ion mode). Peak absorbance at 410 nm requires significantly more than 4 conjugated double bonds,[30] however, so the absorbing conjugated molecule would have to be at least a trimer.

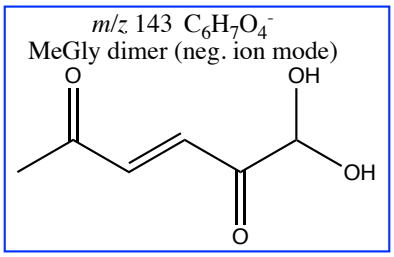

(2)

Methylglyoxal partitioning. The gas-particle partitioning of methylglyoxal can be calculated from the SMPS (particle) and PTR-MS (gas) signals in the eight cloud chamber experiments. Only 4.3 ±1.8% of methylglyoxal remains in the particle phase by the end of each aerosol addition into the chamber at 70 to 80% RH, which is ~4 times lower than in previous studies where methylglyoxal aerosol particles were fully dried.[34, 47] This difference supports the idea that particle drying enhances acetal oligomer formation and retention of α-dicarbonyl compounds in the particle phase. The presence of methylamine, added in the gas or particle phase, did not influence the gas/particle partitioning of methylglyoxal (at 85% or higher confidence levels), consistent with previous studies of aqueous-phase methylamine.[34, 47]

Small chamber experiments: methyglyoxal / AS aerosol + methylamine (g). Now that we have characterized major products, brown carbon production, and viscosity effects in the aerosol phase due to methylamine gas uptake, we next examine the effects of ammonium sulfate and RH on brown carbon production in the methylglyoxal / methylamine reaction system. Methylglyoxal / AS aerosol were characterized by CAPS-ssa before and after exposure to 2 ppm methylamine gas in 7 experiments at 20% RH in a 200L Tedlar chamber (Figure 8, Scheme S2). Before addition of methylamine gas, extinction and scattering declined due to wall losses (except when aerosol dilution in the CAPS inlet was reduced), and albedo also declined, likely due to brown carbon formation by particle-phase methylglyoxal + AS reactions. At 20% RH, browning reactions are

apparently complete within 30 min, and the addition of methylamine gas (t = 0) did not cause any further, long-term aerosol browning. Although extinction and scattering ticked upward when methylamine was added, the increase was not sustained. Concurrent SMPS measurements indicated particle growth of less than 8% by mass upon methylamine addition (Figure S14).

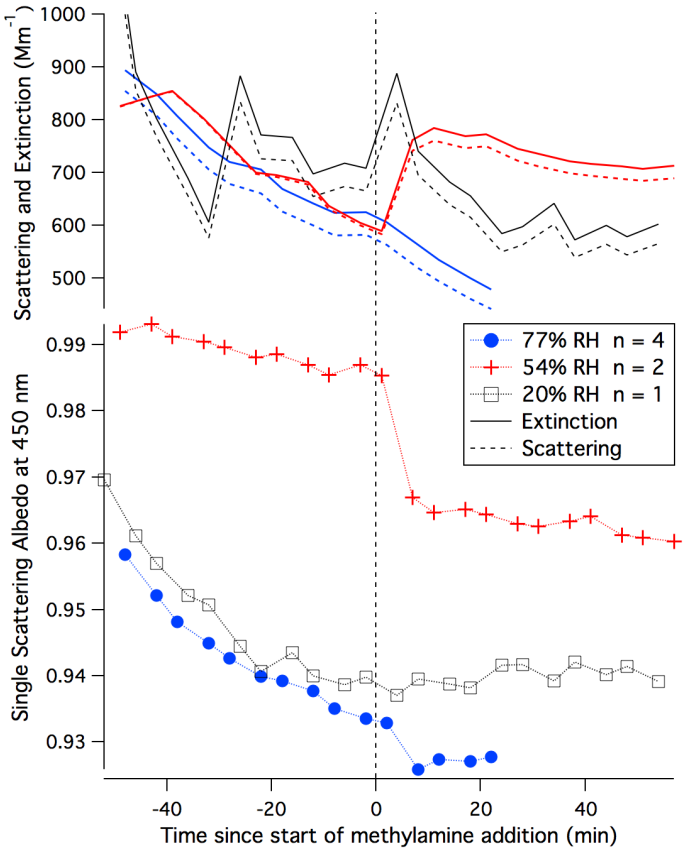

Figure 8: Optical aerosol data from methylglyoxal / AS aerosol + 2 ppm methylamine (g) small chamber experiments. Upper panel: CAPS scattering (dotted lines) and extinction averages (solid lines) for experiments at 20% RH and 0.3 M methylglyoxal / AS aerosol (black), 54% RH and 0.03 M methylglyoxal / AS aerosol (red), and 77% RH and 0.03 M methylglyoxal / AS aerosol (blue), measured at 450 nm immediately after baseline (no particle) zero measurement. Upward jump before methylamine addition in 20% RH experiment is due to an adjustment in aerosol dilution. Lower panel: single-scattering albedo values calculated from data shown in upper panel.

Experiments at higher RH (54% and 77%) were performed with 10× lower methylglyoxal and AS concentrations in the nebulizer (0.03 M instead of 0.3 M). In four experiments at 77% RH, average aerosol albedo initially followed experiments at 20% RH, but albedo dropped by an additional 0.007 after methylamine addition. Aerosol browning upon methylamine addition was even more pronounced at 54% RH, where average albedo dropped by 0.020. Methylamine addition also produced a sustained increase in extinction and scattering at 54% RH, which may indicate growth of the methylglyoxal / AS aerosol particles through methylamine uptake. (Unfortunately, SMPS size distributions are not available in experiments at higher RH.) Analysis of non-time-averaged albedo data from individual runs suggests that browning upon methylamine addition occurred on a timescale consistent with the 1 min mixing time of the chamber. In other words, browning of methylglyoxal / AS aerosol particles upon exposure to methylamine at 54 and 77% RH occurred at the maximum measurable rate.

We can rationalize the different responses of methylglyoxal / AS aerosol to gas-phase methylamine at different RH using what is known about aerosol generated from methylglyoxal / AS solutions. First, AS can effloresce and deliquesce in such particles at RH values that are not far from that of pure AS.[25] Since particles at 20 or 54% RH have been fully dried and then humidified in the chamber to RH levels well below AS deliquescence (79% RH), they will have crystalline AS cores. Moreover, it is known that methylglyoxal / methylamine aerosol forms a semi-solid at RH below 33% RH, while both methylglyoxal / methylamine and methylglyoxal / glycine aerosol begin to take up water at RH above 40%.[25] Thus, at 20% RH it is likely that methylamine gas encounters aerosol consisting of an internal mixture of crystalline AS and semi-solid methylglyoxal oligomers, while at 54% RH the methylglyoxal oligomers may have taken up a substantial amount of water, reducing the viscosity of the organic phase. At 54% RH,

methylamine gas can diffuse into a liquid organic phase and react with methylglyoxal to form light-absorbing products on a timescale of minutes.

At 77% RH, the entire particle should be deliquesced[25] into a single aqueous phase.[48] The drop in albedo before methylamine addition indicates prior brown carbon formation by the methylglyoxal + ammonia reaction (in equilibrium with ammonium sulfate). Methylamine then diffuses into the aqueous particle and reacts with dilute, excess methylglyoxal, causing only a small drop in albedo and not increasing scattering or extinction.

Atmospheric Significance

These studies have demonstrated that exposing methylglyoxal-containing aerosol to ppm-level methylamine gas does not cause measurable particle growth in most experiments, in spite of the high concentration of methylamine used relative to ambient atmospheric concentrations. Nevertheless, chemical, optical and particle bounce measurements indicate that methylamine exposure rapidly forms brown carbon, increases particle viscosity, and initially lowers aerosol hygroscopicity, likely due to the aqueous-phase formation of surface-active, light-absorbing, nitrogen-containing oligomers that are slightly less hygroscopic than the methyglyoxal oligomers they replace. This process is likely analogous to the browning observed when some types of SOA are exposed to indoor ambient levels of ammonia on a filter.[49] Subsequent cloud processing produces cationic imidazole derivatives,[12, 37, 38, 50-52] increasing aerosol hygroscopicity beyond its original level for methylglyoxal aerosol, but without causing additional browning. In simulated sunlight, cloud processing with methylamine dramatically increases particle viscosity, likely due to enhanced aqueous-phase oligomer formation by methylglyoxal photolysis products such as acetyl radicals[30, 53, 54] and hydroxyacetone. These results suggest that the reactive uptake of

methylamine into clouds and aqueous aerosol may influence the optical and physical properties of SOA particles through the conversion of existing oligomers to surface-active, light-absorbing N-containing oligomers and hygroscopic, cationic imidazoles, even as SOA size remains unchanged.

Supporting Information

Experimental schemes, filter reflectance data, small chamber SMPS data, detected ions list, data summaries for experiments 1-2, 4-6, 8, PILS-sampled time-dependent aerosol UV-vis spectra, additional bounce fraction curves vs RH, and PTR-MS calibration curves.

Acknowledgements

This work was funded by NSF grant AGS-1523178. CNRS-INSU is gratefully acknowledged for supporting CESAM as an open facility through the National Instrument label.

References

1. Blando, J. D.; Turpin, B. J., Secondary organic aerosol formation in cloud and fog droplets: a literature evaluation of plausibility. *Atmos. Environ.* **2000,** *34*, 1623-1632. doi:10.1016/S1352-2310(99)00392-1
2. Ervens, B.; Carlton, A. G.; Turpin, B. J.; Altieri, K. E.; Kreidenweis, S. M.; Feingold, G., Secondary organic aerosol yields from cloud-processing of isoprene oxidation products. *Geophys. Res. Lett.* **2008,** *35*, (2), L02816/1-L02816/5. doi:10.1029/2007GL031828
3. Carlton, A. G.; Turpin, B. J.; Altieri, K. E.; Seitzinger, S. P.; Mathur, R.; Roselle, S. J.; Weber, R. J., CMAQ model performance enhanced when in-cloud secondary organic aerosol is included: comparisons of organic carbon predictions with measurements. *Environ. Sci. Technol.* **2008,** *42*, (23), 8798-8802. doi:10.1021/es801192n
4. Dockery, D. W.; Pope, C. A.; Xu, X.; Spengler, J. D.; Ware, J. H.; Fay, M. E.; Ferris, B. G.; Speizer, F. E., An association between air pollution and mortality in six U. S. cities. *N. Engl. J. Med.* **1993,** *329*, (24), 1753-1759. doi:10.1056/NEJM199312093292401
5. IPCC, *Summary for Policymakers*. . Cambridge University Press: Cambridge, United Kingdom and New York, NY, USA, 2013.
6. Ramanathan, V.; Li, F.; Ramana, M. V.; Praveen, P. S.; Kim, D.; Corrigan, C. E.; Nguyen, H.; Stone, E. A.; Schauer, J. J.; Carmichael, G. R.; Adhikary, B.; Yoon, S. C., Atmospheric brown

clouds: hemispherical and regional variations in long-range transport, absorption, and radiative forcing. *J. Geophys. Res.* **2007,** *112*, (D12), D22S21/1-D22S21/26. doi:10.1029/2006JD008124
7. Bahadur, R.; Praveen, P. S.; Xu, Y.; Ramanathan, V., Solar absorption by elemental and brown carbon determine from spectral observations. *Proc. Natl. Acad. Sci. (USA)* **2012,** *109*, (43), 17366-17371. doi:10.1073/pnas.1205910109
8. Feng, Y.; Ramanathan, V.; Kotamarthi, V. R., Brown carbon: a significant atmospheric absorber of solar radiation? *Atmos. Chem. Phys.* **2013,** *13*, (17), 8607-8621. doi:10.5194/acp-13-8607-2013
9. Jo, D. S.; Park, R. J.; Lee, S.; Kim, S. W.; Zhang, X., A global simulation of brown carbon: implications for photochemistry and direct radiative effect. *Atmos. Chem. Phys.* **2016,** *16*, (5), 3413-3432. doi:10.5194/acp-16-3413-2016
10. Shapiro, E. L.; Szprengiel, J.; Sareen, N.; Jen, C. N.; Giordano, M. R.; McNeill, V. F., Light-absorbing secondary organic material formed by glyoxal in aqueous aerosol mimics. *Atmos. Chem. Phys.* **2009,** *9*, 2289-2300. doi:10.5194/acp-9-2289-2009
11. Sareen, N.; Schwier, A. N.; Shapiro, E. L.; Mitroo, D.; McNeill, V. F., Secondary organic material formed by methylglyoxal in aqueous aerosol mimics. *Atmos. Chem. Phys.* **2010,** *10*, 997-1016. doi:10.5194/acp-10-997-2010
12. Yu, G.; Bayer, A. R.; Galloway, M. M.; Korshavn, K. J.; Fry, C. G.; Keutsch, F. N., Glyoxal in aqueous ammonium sulfate solutions: products, kinetics, and hydration effects. *Environ. Sci. Technol.* **2011,** *45*, 6336-6342. doi:10.1021/es200989n
13. Powelson, M. H.; Espelien, B. M.; Hawkins, L. N.; Galloway, M. M.; De Haan, D. O., Brown carbon formation by aqueous-phase aldehyde reactions with amines and ammonium sulfate. *Environ Sci Technol* **2014,** *48*, (2), 985-993. doi:10.1021/es4038325
14. Lin, P.; Laskin, J.; Nizkorodov, S. A.; Laskin, A., Revealing Brown Carbon Chromophores Produced in Reactions of Methylglyoxal with Ammonium Sulfate. *Environ Sci Technol* **2015,** *49*, (24), 14257-14266. doi:10.1021/acs.est.5b03608
15. Laskin, A.; Laskin, J.; Nizkorodov, S. A., Chemistry of Atmospheric Brown Carbon. *Chem. Rev.* **2015,** *115*, 4335-4382. doi:10.1021/cr5006167
16. Igawa, M.; Munger, J. W.; Hoffmann, M. R., Analysis of aldehydes in cloud- and fogwater samples by HPLC with a postcolumn reaction detector. *Environ. Sci. Technol.* **1989,** *23*, (5), 556-561. doi:10.1021/es00063a007
17. Munger, J. W.; Jacob, D. J.; Daube, B. C.; Horowitz, L. W.; Keene, W. C.; Heikes, B. G., Formaldehyde, glyoxal, and methylglyoxal in air and cloudwater at a rural mountain site in central Virginia. *J. Geophys. Res.* **1995,** *100*, (D5), 9325-9333. doi:10.1029/95JD00508
18. Matsumoto, K.; Kawai, S.; Igawa, M., Dominant factors controlling concentrations of aldehydes in rain, fog, dew water, and in the gas phase. *Atmos. Environ.* **2005,** *39*, 7321-7329. doi:10.1016/j.atmosenv.2005.09.009
19. Wittrock, F.; Richter, A.; Oetjen, H.; Burrows, J. P.; Kanakidou, M.; Myriokefalitakis, S.; Volkamer, R.; Beirle, S.; Platt, U.; Wagner, T., Simultaneous global observations of glyoxal and formaldehyde from space. *Geophys. Res. Lett.* **2006,** *33*, L16804. doi:10.1029/2006GL026310
20. Zhang, Q.; Anastasio, C., Chemistry of fog waters in California's Central Valley -- Part 3: Concentrations and speciation of organic and inorganic nitrogen. *Atmos. Environ.* **2001,** *35*, 5629-5643. doi:10.1016/S1352-2310(01)00337-5

21. Ge, X.; Wexler, A. S.; Clegg, S. L., Atmospheric amines – Part I. A review. *Atmos. Environ.* **2011,** *45*, (3), 524-546. doi:https://doi.org/10.1016/j.atmosenv.2010.10.012
22. Wang, Y.; Zhang, J.; Marcotte, A. R.; Karl, M.; Dye, C.; Herckes, P., Fog chemistry at three sites in Norway. *Atmos. Res.* **2015,** *151*, 72-81. doi:10.1016/j.atmosres.2014.04.016
23. De Haan, D. O.; Corrigan, A. L.; Smith, K. W.; Stroik, D. R.; Turley, J. T.; Lee, F. E.; Tolbert, M. A.; Jimenez, J. L.; Cordova, K. E.; Ferrell, G. R., Secondary organic aerosol-forming reactions of glyoxal with amino acids. *Environ. Sci. Technol.* **2009,** *43*, (8), 2818-2824. doi:10.1021/es803534f
24. De Haan, D. O.; Hawkins, L. N.; Welsh, H. G.; Pednekar, R.; Casar, J. R.; Pennington, E. A.; de Loera, A.; Jimenez, N. G.; Symons, M. A.; Zauscher, M.; Pajunoja, A.; Caponi, L.; Cazaunau, M.; Formenti, P.; Gratien, A.; Pangui, E.; Doussin, J. F., Brown carbon production in ammonium- or amine-containing aerosol particles by reactive uptake of methylglyoxal and photolytic cloud cycling. *Environ Sci Technol* **2017,** *51*, (13), 7458-7466. doi:10.1021/acs.est.7b00159
25. Hawkins, L. N.; Baril, M. J.; Sedehi, N.; Galloway, M. M.; De Haan, D. O.; Schill, G. P.; Tolbert, M. A., Formation of semi-solid, oligomerized aqueous SOA: Lab simulations of cloud processing. *Environ Sci Technol* **2014,** *48*, (4), 2273-2280. doi:10.1021/es4049626
26. Updyke, K. M.; Nguyen, T. B.; Nizkorodov, S. A., Formation of brown carbon via reactions of ammonia with secondary organic aerosols from biogenic and anthropogenic precursors. *Atmos. Environ.* **2012,** *63*, 22-31. doi:10.1016/j.atmosenv.2012.09.012
27. Wang, J.; Doussin, J. F.; Perrier, S.; Perraudin, E.; Katrib, Y.; Pangui, E.; Picquet-Varrault, B., Design of a new multi-phase experimental simulation chamber for atmospheric photosmog, aerosol and cloud chemistry research. *Atmos. Meas. Tech.* **2011,** *4*, 2465-2494. doi:10.5194/amt-4-2465-2011
28. Pajunoja, A.; Lambe, A. T.; Hakala, J.; Rastak, N.; Cummings, M. J.; Brogan, J. F.; Hao, L.; Paramonov, M.; Hong, J.; Prisle, N. L.; Malila, J.; Romakkaniemi, S.; Lehtinen, K. E. J.; Laaksonen, A.; Kulmala, M.; Massoli, P.; Onasch, T. B.; Donahue, N. M.; Riipinen, I.; Davidovits, P.; Worsnop, D. R.; Petäjä, T.; Virtanen, A., Adsorptive uptake of water by semisolid secondary organic aerosols. *Geophys. Res. Lett.* **2015,** *42*, (8), 3063-3068. doi:10.1002/2015GL063142
29. Brégonzio-Rozier, L.; Giorio, C.; Siekmann, F.; Pangui, E.; Morales, S. B.; Temime-Roussel, B.; Gratien, A.; Michoud, V.; Cazaunau, M.; DeWitt, H. L.; Tapparo, A.; Monod, A.; Doussin, J. F., Secondary organic aerosol formation from isoprene photooxidation during cloud condensation–evaporation cycles. *Atmos. Chem. Phys.* **2016,** *16*, (3), 1747-1760. doi:10.5194/acp-16-1747-2016
30. De Haan, D. O.; Tapavicza, E.; Riva, M.; Cui, T.; Surratt, J.; Smith, A. C.; Jordan, M.-C.; Nilakantan, S.; Almodovar, M.; Stewart, T. N.; de Loera, A.; De Haan, A. C.; Cazaunau, M.; Gratien, A.; Pangui, E.; Doussin, J. F., Nitrogen-containing, light-absorbing oligomers produced in aerosol particles exposed to methylglyoxal, photolysis, and cloud cycling. *Environ. Sci. Technol.* **2018,** *52*, (7), 4061-4071. doi:10.1021/acs.est.7b06105
31. Lee, A. K. Y.; Zhao, R.; Li, R.; Liggio, J.; Li, S.-M.; Abbatt, J. P. D., Formation of light absorbing organo-nitrogen species from evaporation of droplets containing glyoxal and ammonium sulfate. *Environ Sci Technol* **2013,** *47*, (22), 12819-12826. doi:10.1021/es402687w
32. Davidek, T.; Velisek, J.; Davidek, J.; Pech, P., Amino acids derived 1,3-disubstituted imidazoles in nonenzymatic browning reactions. *Sbornik Vysoke Skoly Chemicko-Technologicke v Praze, E: Potraviny* **1991,** *62*, 165-182.

33. Büchi, G.; Demole, E.; Thomas, A. F., Synthesis of 2,5-dimethyl-4-hydroxy-2,3-dihydrofuran-3-one (furaneol), a flavor principle of pineapple and strawberry. *J. Org. Chem.* **1973,** *38*, (1), 123-125. doi:10.1021/jo00941a025
34. De Haan, D. O.; Corrigan, A. L.; Tolbert, M. A.; Jimenez, J. L.; Wood, S. E.; Turley, J. J., Secondary organic aerosol formation by self-reactions of methylglyoxal and glyoxal in evaporating droplets. *Environ. Sci. Technol.* **2009,** *43*, (21), 8184-8190. doi:10.1021/es902152t
35. Yasmeen, F.; Sauret, N.; Gal, J. F.; Maria, P. C.; Massi, L.; Maenhaut, W.; Claeys, M., Characterization of oligomers from methylglyoxal under dark conditions: a pathway to produce secondary organic aerosol through cloud processing during nighttime. *Atmos. Chem. Phys.* **2010,** *10*, (8), 3803-3812. doi:10.5194/acp-10-3803-2010
36. Velisek, J.; Davidek, T.; Davidek, J.; Trska, P.; Kvasnicka, F.; Velcova, K., New imidazoles formed in nonenzymatic browning reactions. *J. Food Sci.* **1989,** *54*, (6), 1544-1546. doi:10.1111/j.1365-2621.1989.tb05155.x
37. Galloway, M. M.; Chhabra, P. S.; Chan, A. W. H.; Surratt, J. D.; Flagan, R. C.; Seinfeld, J. H.; Keutsch, F. N., Glyoxal uptake on ammonium sulphate seed aerosol: reaction products and reversibility of uptake under dark and irradiated conditions. *Atmos. Chem. Phys.* **2009,** *9*, 3331-3345. doi:10.5194/acp-9-3331-2009
38. De Haan, D. O.; Hawkins, L. N.; Kononenko, J. A.; Turley, J. J.; Corrigan, A. L.; Tolbert, M. A.; Jimenez, J. L., Formation of nitrogen-containing oligomers by methylglyoxal and amines in simulated evaporating cloud droplets. *Environ. Sci. Technol.* **2011,** *45*, (3), 984-991. doi:10.1021/es102933x
39. Teich, M.; van Pinxteren, D.; Kecorius, S.; Wang, Z.; Herrmann, H., First quantification of imidazoles in ambient aerosol particles: Potential photosensitizers, brown carbon constituents, and hazardous components. *Environ Sci Technol* **2016,** *50*, 1166-1173. doi:10.1021/acs.est.5b05474
40. Saukko, E.; Lambe, A. T.; Massoli, P.; Koop, T.; Wright, J. P.; Croasdale, D. R.; Pedernera, D. A.; Onasch, T. B.; Laaksonen, A.; Davidovits, P.; Worsnop, D. R.; Virtanen, A., Humidity-dependent phase state of SOA particles from biogenic and anthropogenic precursors. *Atmos. Chem. Phys.* **2012,** *12*, 7517-7529. doi:10.5194/acp-12-7517-2012
41. Pajunoja, A.; Hu, W.; Leong, Y. J.; Taylor, N. F.; Miettinen, P.; Palm, B. B.; Mikkonen, S.; Collins, D. R.; Jimenez, J. L.; Virtanen, A., Phase state of ambient aerosol linked with water uptake and chemical aging in the southeastern US. *Atmos. Chem. Phys.* **2016,** *16*, (17), 11163-11176. doi:10.5194/acp-16-11163-2016
42. Sander, R., Compilation of Henry's law constants (version 4.0) for water as solvent. *Atmos. Chem. Phys.* **2015,** *15*, 4399-4981. doi:10.5194/acp-15-4399-2015
43. Lee, H. J.; Aiona, P. K.; Laskin, A.; Laskin, J.; Nizkorodov, S. A., Effect of solar radiation on the optical properties and molecular composition of laboratory proxies of atmospheric brown carbon. *Environ. Sci. Technol.* **2014,** *48*, (17), 10217-10226. doi:10.1021/es502515r
44. Aiona, P. K.; Lee, H. J.; Leslie, R.; Lin, P.; Laskin, A.; Laskin, J.; Nizkorodov, S. A., Photochemistry of Products of the Aqueous Reaction of Methylglyoxal with Ammonium Sulfate. *ACS Earth and Space Chemistry* **2017,** *1*, (8), 522-532. doi:10.1021/acsearthspacechem.7b00075
45. Wong, J. P. S.; Nenes, A.; Weber, R. J., Changes in Light Absorptivity of Molecular Weight Separated Brown Carbon Due to Photolytic Aging. *Environ Sci Technol* **2017,** *51*, (15), 8414-8421. doi:10.1021/acs.est.7b01739

46. Nemet, I.; Vikic-Topic, D.; Varga-Defterdarovic, L., Spectroscopic studies of methylglyoxal in water and dimethylsulfoxide. *Bioorg. Chem.* **2004,** *32*, 560-570. doi:10.1016/j.bioorg.2004.05.008
47. Galloway, M. M.; Powelson, M. H.; Sedehi, N.; Wood, S. E.; Millage, K. D.; Kononenko, J. A.; Rynaski, A. D.; De Haan, D. O., Secondary organic aerosol formation during evaporation of droplets containing atmospheric aldehydes, amines, and ammonium sulfate. *Environ Sci Technol* **2014,** *48*, 14417-14425. doi:10.1021/es5044479
48. Bertram, A. K.; Martin, S. T.; Hanna, S. J.; Smith, M. L.; Bodsworth, A.; Chen, Q.; Kuwata, M.; Liu, A.; You, Y.; Zorn, S. R., Predicting the relative humidities of liquid-liquid phase separation, efflorescence, and deliquescence of mixed particles of ammonium sulfate, organic material, and water using the organic-to-sulfate mass ratio of the particle and the oxygen-to-carbon elemental ratio of the organic component. *Atmos. Chem. Phys.* **2011,** *11*, 10995-11006. doi:10.5194/acp-11-10995-2011
49. Bones, D. L.; Henricksen, D. K.; Mang, S. A.; Gonsior, M.; Bateman, A. P.; Nguyen, T. B.; Cooper, W. J.; Nizkorodov, S. A., Appearance of strong absorbers and fluorophores in limonene-O_3 secondary organic aerosol due to NH_4^+-mediated chemical aging over long time scales. *J. Geophys. Res. - Atmos.* **2010,** *115*, (D5), D05203/1-14. doi:10.1029/2009JD012864
50. Galloway, M. M.; Loza, C. L.; Chhabra, P. S.; Chan, A. W. H.; Yee, L. D.; Seinfeld, J. H.; Keutsch, F. N., Analysis of photochemical and dark glyoxal uptake: Implications for SOA formation. *Geophys. Res. Lett.* **2011,** *38*. doi: 10.1029/2011GL048514
51. Kampf, C. J.; Jakob, R.; Hoffmann, T., Identification and characterization of aging products in the glyoxal/ammonium sulfate system -- implications for light-absorbing material in atmospheric aerosols. *Atmos. Chem. Phys.* **2012,** *12*, 6323-6333. doi:10.5194/acp-12-6323-2012
52. Maxut, A.; Noziere, B.; Fenet, B.; Mechakra, H., Formation mechanisms and yields of small imidazoles from reactions of glyoxal with NH4+ in water at neutral pH. *Phys. Chem. Chem. Phys.* **2015,** *17*, (31), 20416-20424. doi:10.1039/C5CP03113C
53. Chen, Y.; Wang, W.; Zhu, L., Wavelength-Dependent Photolysis of Methylglyoxal in the 290–440 nm Region. *The Journal of Physical Chemistry A* **2000,** *104*, (47), 11126-11131. doi:10.1021/jp002262t
54. Atkinson, R.; Baulch, D. L.; Cox, R. A.; Crowley, J. N.; Hampson, R. F.; Hynes, R. G.; Jenkin, M. E.; Rossi, M. J.; Troe, J., Evaluated kinetic and photochemical data for atmospheric chemistry: Volume II - gas phase reactions of organic species. *Atmos. Chem. Phys.* **2006,** *6*, (11), 3625-4055. doi:10.5194/acp-6-3625-2006

TOC art

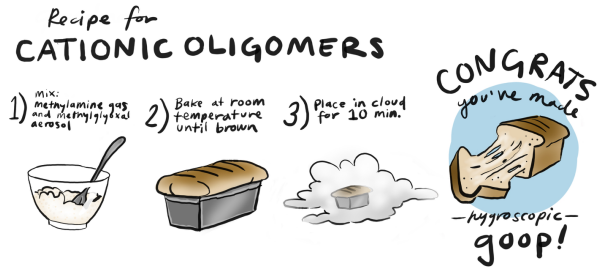
Recipe for
CATIONIC OLIGOMERS
1) Mix: methylamine gas and methylglyoxal aerosol
2) Bake at room temperature until brown
3) Place in cloud for 10 min.
CONGRATS you've made
-hygroscopic-
goop!